um hexafluorophosphate solutions, using freshly distilled tetrahydrofuran or methylene chloride. All solutions were prepared under an atmosphere of nitrogen and degassed completely before injection into the SEC cell. Blank reference solutions containing 0.1 M tetra-*n*-butyl ammonium hexafluorophosphate were used for the Fourier transform IR solvent subtractions. A Princeton Applied Research (PAR) model 175 Universal Programmer with a PAR model 176 Current Follower were used to effect and monitor thin-layer bulk electrolyses. The IR spectra were acquired with a Mattson Research Series Fourier transform IR equipped with a MCT (mercury-cadmium-telluride) detector.
23. R. E. Wittrig and C. P. Kubiak, *J. Electroanal. Chem.* **393**, 75 (1995).
24. F.-W. Grevels *et al.*, *Angew. Chem. Int. Ed. Engl.* **26**, 885 (1987).
25. H. L. Strauss, *J. Am. Chem. Soc.* **114**, 905 (1992).
26. J. J. Turner, C. M. Gordon, S. M. Howdle, *J. Phys. Chem.* **99**, 17532 (1995).
27. M. Eigen, *Angew. Chem. Int. Ed. Engl.* **3**, 1 (1964).
28. B. Cohen and S. Weiss, *J. Phys. Chem.* **87**, 3606 (1983).
29. R. A. MacPhail and H. L. Strauss, *J. Chem. Phys.* **82**, 1156 (1985).
30. S. Bratos, G. Tarjus, P. Viot, *ibid.* **85**, 803 (1986).
31. S. Mazur, C. Sreekumar, A. H. Schroeder, *J. Am. Chem. Soc.* **98**, 6713 (1976).
32. A. H. Schroeder and S. Mazur, *ibid.* **100**, 7339 (1978).
33. G. M. Tom and H. Taube, *ibid.* **97**, 5310 (1975).
34. F. Coat and C. Lapinte, *Organometallics* **15**, 477 (1996).
35. R. H. Magnuson and H. Taube, *J. Am. Chem. Soc.* **94**, 7213 (1972).
36. H. Krentzien and H. Taube, *ibid.* **98**, 6379 (1976).
37. M. B. Sponsler, *Organometallics* **14**, 1920 (1995).
38. R. Wu *et al.*, *J. Chem. Soc. Chem. Commun.* **1994**, 1657 (1994).
39. K. A. Wood and H. L. Strauss, *J. Phys. Chem.* **94**, 5677 (1990).
40. A. E. Johnson and A. B. Meyers, *ibid.* **100**, 7778 (1996).
41. IR spectral lineshapes were simulated with the dynamical simulation program VIBEXGL: Program for the Simulation of IR Spectra of Exchanging Systems, made available by R. E. D. McClung, University of Alberta, Alberta, Canada.
42. Supported by NSF grants (CHE-9319173 and CHE-9615886) to C.P.K. and Grants-in-Aid for Scientific Research (08243214 and 09874128) from the Ministry of Education, Science, and Culture and by a grant from Monbusho International Scientific Research Program (No. 09044054) (Japan) to T.I. We also gratefully acknowledge the Japan Society for the Promotion of Science for fellowship support to C.P.K. and Natural Sciences and Engineering Research Council (Canada) for a postdoctoral fellowship to J.W.

25 March 1997; accepted 9 June 1997

An Advective-Reflective Conceptual Model for the Oscillatory Nature of the ENSO

J. Picaut,* F. Masia, Y. du Penhoat†

Recent findings about zonal displacements of the Pacific warm pool required a notable modification of the delayed action oscillator theory, the current leading theory for the El Niño–Southern Oscillation (ENSO). Simulations with a linearized coupled ocean-atmosphere model resulted in 3- to 6-year ENSO-like oscillations, with many of the variable model parameters found to be very close to their observed values. This simple model suggests that ocean processes that are ignored or underestimated in the delayed action oscillator theory, such as zonal current convergence, zonal advection of sea surface temperature, and equatorial wave reflection from the eastern ocean boundary, are fundamental to the development of the ENSO, in particular to its manifestations in the central equatorial Pacific.

Earth climate variations on interannual time scales are dominated by a coupled ocean-atmosphere interaction in the Pacific. This interaction connects a large-scale oceanic sea surface temperature (SST) anomaly of the tropical Pacific (El Niño) to the large-scale atmospheric Southern Oscillation, which is characterized by a sea-level pressure seesaw between French Polynesia and north Australia [defined by the Southern Oscillation Index (SOI)]. This coupled phenomenon, named the ENSO, oscillates irregularly (roughly every 4 years) into a warm phase and a cold phase (Fig. 1). The warm phase, El Niño, is characterized by warm SST and weak easterly winds in the central and eastern equatorial Pacific, energetic westerly winds in the western Pacific, and negative SOI; whereas the cold phase, La Niña, is characterized by cold SST and strong easterly winds in the central and eastern equatorial Pacific, weak westerly winds in the western Pacific, and positive SOI. The gross features of the ENSO, and some of its dramatic climatic impacts, can be predicted 6 months to a year in advance by dynamical coupled ocean-atmosphere models (*1*–*3*). However, the prediction skills of these models are still limited by our insufficient understanding of the intrinsic mechanism that is responsible for the ENSO.

Bjerknes (*4*) proposed that the ENSO is a self-sustained system in which SST variations in the eastern and central equatorial Pacific produce wind variations, which in turn produce SST changes. However, this scenario leads to a never ending warm or cold state. A mechanism for the oscillatory nature of the ENSO was originally proposed by McCreary (*5*), based on the reflection of a subtropical oceanic upwelling Rossby wave against the western ocean boundary. Battisti, Hirst, Schopf, and Suarez (*6*–*8*) proposed a concept that was similar to McCreary's (but was better supported by observations and equatorial wave theory), known as the delayed action oscillator, in which equatorial Rossby waves reflected as upwelling equatorial Kelvin waves are essential (*9*). Given the 9-month total travel time of the equatorial upwelling Rossby and reflected Kelvin waves, this concept asserts that it is the continuous arrival of upwelling Kelvin waves that slowly erodes the growing SST-wind interaction in the eastern equatorial Pacific, finally stops it after 1 or 2 years, and eventually turns the El Niño event into a La Niña event.

The delayed action oscillator theory is currently the leading theory for the ENSO, although it has several flaws. First, the maxima in the coupled SST–wind stress fields, simulated by the different models that led to this theory, are located 20° to 40° too far into the eastern equatorial Pacific as compared with observations (Fig. 1) (*10*). Second, on the basis of mooring data all along the equatorial Pacific and satellite altimetry data, several authors have questioned the effectiveness of the western ocean boundary as an equatorial wave reflector (*11*–*14*). In contrast, it seems that equatorial Kelvin waves reflect quite well on the eastern boundary as equatorial Rossby waves (*14*). Third, the models that have led to this theory of the ENSO are based on the dominant role of thermocline displacements on SST in the eastern equatorial Pacific, and they underestimate or misinterpret the effects of zonal advection (*15*). As a result, these models consider the eastern equatorial Pacific (where ENSO-related SST variations are the strongest) to be the source of the ENSO air-sea interaction, instead of the central equatorial Pacific (Fig. 1) (*10*).

The central equatorial Pacific has been confirmed as the source of the ENSO in recent studies (*16*–*19*), which indicated that the central equatorial Pacific SST varies between 26° and 30°C, predominantly on the ENSO time scale, as a result of the strong eastward and westward displacements of the eastern edge of the western Pacific warm pool. Because the SST varies around the approximate 28°C

Groupe SURTROPAC, L'Institut Français de Recherche Scientifique pour le Développement en Coopération–ORSTOM, BP A5, 98848, Nouméa, New Caledonia.

*To whom correspondence should be addressed. E-mail: picaut@noumea.orstom.nc
†Present address: Groupe de Recherche en Géodésie Spatiale, 14 avenue Edouard Belin, 31401, Toulouse, France.

threshold required for the maintenance of organized atmospheric convection, the central equatorial Pacific is at the origin of the dominant mode of ENSO coupled ocean-atmosphere variability on a global scale (Fig. 1) (*17*). The dominance of zonal advection in these zonal displacements was demonstrated in several of these studies. This was supported by the discovery of a zone of convergence of water masses into a well-defined salinity front that moves together with the eastern edge of the warm pool, eastward and westward during the El Niño and La Niña phases, respectively (Fig. 1) (*19*). The oceanic convergence zone is due to the confluence, within the equatorial wave guide (*20*), of sporadic currents from the west and nearly continuous currents from the east (*19, 21*). The zonal displacements of the oceanic convergence zone–eastern edge of the warm pool (hereafter referred to as OCEE) are therefore predominantly governed by the variations of zonal surface currents generated by the combined effects of (i) local wind forcing (Fig. 1B), (ii) free equatorial Kelvin and first meridional mode Rossby waves, and (iii) reflected equatorial waves on the western and eastern ocean boundaries. In particular, it appears from observations that the eastern boundary reflection of a downwelling Kelvin wave into a first meridional mode downwelling Rossby wave may have been responsible for the shift of the 1986–87 El Niño into the 1988–89 La Niña (*18*). Therefore we propose a concept for the oscillatory nature of the ENSO that can be considered a significant modification of the delayed action oscillator theory, with an important role played by zonal advection and equatorial wave reflection on the eastern ocean boundary.

This concept can be illustrated with a simple ocean-atmosphere coupled model, based on recent in situ and satellite observations. A linear wind-forced ocean model, derived from a low-frequency, long-wave, approximation model (*22*), was restricted to the zonal current of the first baroclinic Kelvin and first meridional Rossby modes (*20, 23*). The ocean model did not simulate SST, and the location of the oceanic zone of convergence was used as a surrogate for the location of the eastern edge of the warm pool (*24*). As in a previous study (*19*), the location of the OCEE was determined by the trajectory of a hypothetical drifter moving with the average zonal currents within the equatorial band. In the present study, this band was usually set to 2°N to 2°S, and the zonal currents were calculated as the sum of the modeled varying currents and the mean currents (Fig. 2). The atmospheric forcing and the coupling principle used in the model were based on a simple approximation of the observed SST and wind

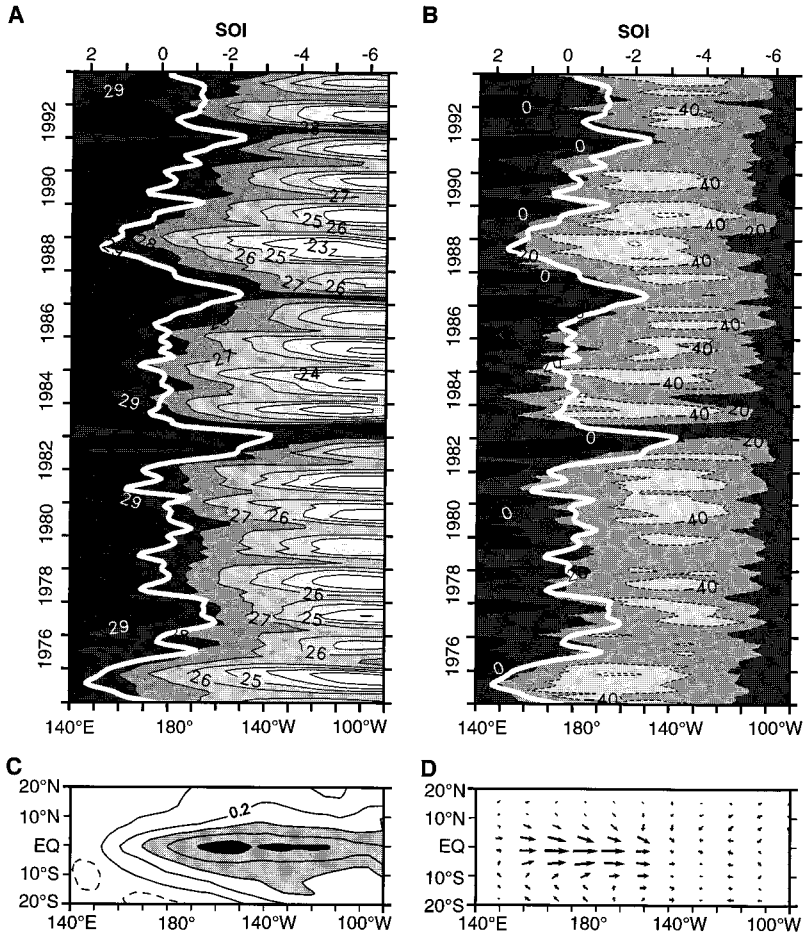

Fig. 1. Longitude-time distribution of the 2°N to 2°S averaged (**A**) SST (contour is every 1°C) and (**B**) zonal pseudo wind stress (contour is every 20 m^2 s^{-2}). Superimposed as a thick white line is the SOI. All series are low-pass filtered to suppress oscillations of periods shorter than 3 months. Dominant mode of ENSO covariability of the (**C**) SST and (**D**) pseudo vector wind stress over the 1975–93 period. The SST contour is every 0.2°C, and a sample of 5 m^2 s^{-2} vector wind stress is included for scale [adapted from (*10*)]. EQ, equator.

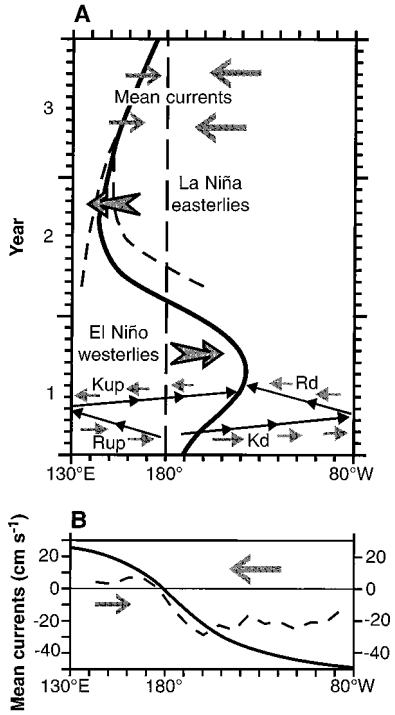

Fig. 2. Concept of the reflective-advective coupled system: (**A**) Longitude-time distribution within 2°N to 2°S of the common OCEE of the warm pool (thick line). Superimposed are the schematic representations of the equatorial Kelvin (Kup and Kd for upwelling and downwelling, respectively) and first meridional mode Rossby wave (Rup and Rd for upwelling and downwelling, respectively) propagating paths (lines with small dark arrows) and their associated zonal currents (small gray arrows), the mean zonal converging currents, and the westerly and easterly winds. Also shown is an example of two drifters converging into the OCEE of the warm pool (*19*). (**B**) Longitude distribution of the mean zonal currents (in centimeters per second) averaged within 2°N to 2°S deduced from observations (dashed line) and schematized for this model (thick line).

interaction in the central and western equatorial Pacific (Fig. 1). During El Niño, westerly winds penetrate from the western equatorial Pacific into the central equatorial Pacific simultaneously with the eastward displacement of the eastern edge of the warm pool. The pattern is reversed during La Niña. Atmospheric model simulations (*25*) and Fig. 1B suggest that the amplitude of the penetrating winds is fairly independent of the extent of penetration. The anomalous zonal wind stress that forced the ocean model was therefore defined as a patch of wind of constant amplitude whose zonal extent varied simultaneously with the zonal displacement of the eastern edge of the warm pool (*26*). This zonal extent was proportional to the distance between the instantaneous position of the OCEE and the mean climatologic position of the OCEE [hereafter called the "midpoint" and situated around 180° (Figs. 1 and 2) (*27*)].

In this model (Fig. 2A), at initial time (t = 0 month), a westerly wind patch is applied (*28*), and it induces local zonal currents that advect the OCEE toward the east against the weaker mean zonal current. At the same time, downwelling Kelvin waves and upwelling Rossby waves, on each side of the wind patch, propagate eastward and westward, respectively. The wind patch expands eastward simultaneously with the displacement of the OCEE and generates local currents and equatorial waves of greater amplitude. As a consequence, the displacement of the OCEE accelerates and El Niño enters into a growth phase. It is the combination of two sets of zonal currents, in opposite direction to the original wind-forced currents, that gradually reduces the acceleration of the eastward progression of the OCEE. One set is produced by the delayed arrival of the reflected equatorial waves from both ocean boundaries (Fig. 2A); the other corresponds to the mean zonal current that, as shown on Fig. 2B, increases in strength concurrently with the eastward displacement of the OCEE. Eventually, this combination stops the OCEE displacement toward the east ($t \sim 8$ months) and finally pushes it back toward the midpoint. Once the midpoint is crossed, the wind shifts from westerly to easterly (*27*) and El Niño turns into La Niña ($t \sim 13$ months); then La Niña turns into El Niño ($t \sim 39$ months) and the ENSO phases repeat indefinitely.

The model includes several parameters, and numerous sensitivity calculations were done to determine the ranges of parameters that result in an ENSO-like oscillation of the model. We defined a "standard case," in which all parameters were set very close to their mean values (*29*). It resulted (Fig. 3, curve b) in a lopsided oscillation (that is, a longer time to go into an El Niño than into a La Niña) with a 4-year period and an amplitude of 25° (defined as half the distance from the crest to the trough). The simulation resembled the observed ENSO (Fig. 1), which has on average a 3.8-year period (*30*) and a lopsided pattern. The sensitivity calculations are summarized on Fig. 4, where one parameter at a time was changed, while the others were kept fixed at their standard case values. The equatorial Kelvin wave-speed range corresponded to the first baroclinic mode and was found to be very close to the one determined from in situ and satellite observations (Fig. 4A) (*13, 31*). The location of the midpoint (mean OCEE) ranged around the observed value of 180° (Figs. 1 and 4B). The latitudinal trapping remained close to the observed value of 7° (Figs. 1D and 4C). A close look at Fig. 1 suggests a 5° to 15° longitudinal shift between the eastern edge of the warm pool and that of the wind patch (Fig. 4D). The amplitude of the wind stress had a narrow range around 0.33 dynes cm^{-2} which fell into the 0.20 to 0.40 dynes cm^{-2} range of observed ENSO wind stress anomalies (Fig. 4E) (*15*). Many ocean modelers use 2.5 year^{-1} for the Rayleigh friction. Comparisons with observations (*32*) suggest a friction of 6 month^{-1} for the first baroclinic mode, and the present sensitivity experiment implied the use of friction smaller than 1.5 year^{-1} (Fig. 4F). A series of tests (*33*) indicated a rather limited north-south extension for the width of the equatorial band over which the zonal currents are averaged to displace the OCEE (within 1.75°N to 1.75°S and 2.25°N to 2.25°S). A previous study (*18*) based on observations did not find a substantial change in OCEE displacements when the zonal currents were averaged within 2°N to 2°S and 6°N to 6°S. The final test considered different values for the mean zonal current near the western and eastern ocean boundaries (Fig. 2B). It appears to be difficult to get the model to oscillate for values below 15 cm s^{-1} near the western boundary and above −35 cm s^{-1} near the eastern boundary. These numbers are still too large compared with those of the observations (*34*).

As discussed above, an important and controversial question about the delayed action oscillator theory compared with the present approach is the effectiveness of the western and eastern ocean boundaries as equatorial wave reflectors. Several simulations were done with our model, with

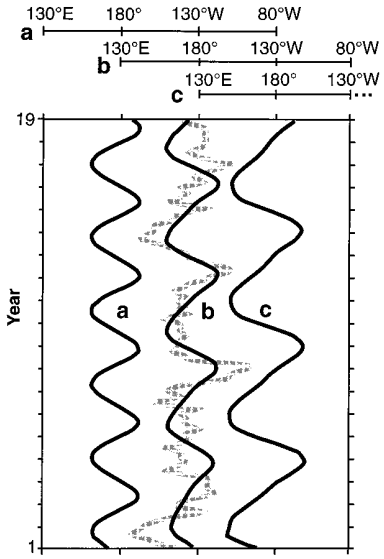

Fig. 3. Examples of a 19-year simulation with various reflection coefficients: Ten percent reflection coefficient on the western boundary and 100% reflection coefficient on the eastern boundary (curve a). Standard case, with 100% reflection coefficient on the western and eastern boundaries (curve b). Ninety percent reflection coefficient on the eastern boundary and 100% reflection coefficient on the western boundary (curve c). The curves are shifted by 50° longitude for clarity. Superimposed on curve b as a thick gray curve is the SOI of Fig. 1 over the 19-year period from 1975 to 1993.

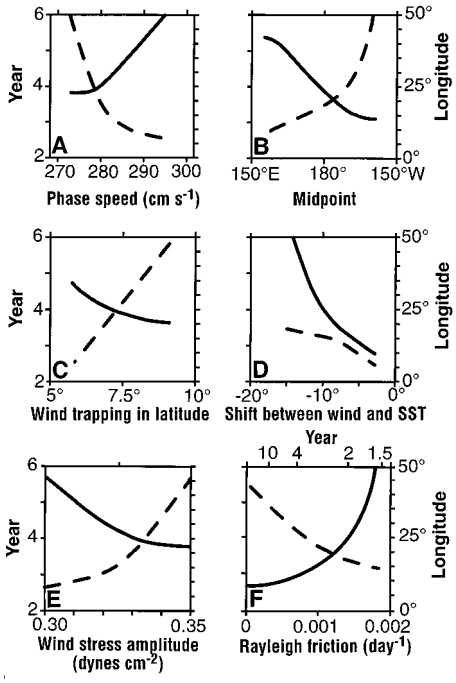

Fig. 4. Period (solid lines) and amplitude (dashed lines) of the ENSO oscillation obtained from the variation of a specific parameter, with all other parameters set to the standard case. (**A**) Phase speed. (**B**) Location of the midpoint. (**C**) Wind trapping in latitude. (**D**) Shift between wind and SST. (**E**) Wind stress amplitude. (**F**) Rayleigh friction.

the addition of reflection coefficients on both boundaries. It is possible to get ENSO-like oscillations with no or very little (<10%) western boundary reflection, through a reduction of the wind stress amplitude (Fig. 3, curve a). In contrast, it is impossible to obtain ENSO-like oscillations with a reflection coefficient on the eastern boundary that is smaller than 85% (Fig. 3, curve c).

Despite its simplicity, the proposed coupled model is adequate to illustrate the advective-reflective concept for the oscillatory nature of the ENSO. Many of the parameters that yielded realistic simulations of the ENSO were found to be surprisingly close to their observed values. The concept is based on the discovery of the OCEE that is advected in phase with the SOI (*19*); as a consequence, the ENSO time scale can be accurately determined by the duration of advection of the eastern edge of the warm pool by surface zonal currents in the equatorial band. This is more direct than the estimation proposed by recent ENSO theories, based on the time taken by some negative feedback to stop the unstable growth of the coupled system. However, our model results in regular oscillations, and as seen on Figs. 1 and 3, curve b, the ENSO is subject to strong irregularities. This could be due to the fact that several parameters that were treated as constants in the model are not really constant in nature (such as Kelvin wave speed and wind amplitude). These irregularities are beyond the scope of the present study.

The present model requires stronger than observed mean zonal converging currents (Fig. 2B), very likely to compensate for the simplified model physics, such as the exclusion of nonlinear terms and of vertical advection for changing SST. During the fully developed El Niño, when warm waters stretch well into the eastern equatorial Pacific, the zonal SST gradient on the eastern edge of the warm pool does not remain nearly constant but weakens significantly (Fig. 1A). Zonal advection associated with the returning displacement of the OCEE does not bring cold SST into the central equatorial Pacific, and a source of cold water is needed in the eastern equatorial Pacific to develop a La Niña. Heat flux contributions to SST variations are not very substantial within the equatorial wave guide on an ENSO time scale (*35*); thus, uplifting of the thermocline appears to be the most likely mechanism for this source. With the returning surface westward flow, mass conservation along the equatorial wave guide ensures an uplifting of the thermocline in the eastern equatorial Pacific (*36*). In this case, our concept is pertinent during both phases of the ENSO. On the other hand, the uplifting of the thermocline can also be accounted for by the original delayed action theory through the action of reflected upwelling Kelvin waves issued from the western ocean boundary. In this second case, our concept is relevant during La Niña and much of the duration of El Niño. Hence, as a modification of the delayed action oscillator theory, we propose a concept in which equatorial wave reflection on the eastern boundary is more important than on the western boundary and zonal advection is more effective overall than vertical advection and entrainment for setting up the coupled ENSO system in the right place, namely, in the central equatorial Pacific.

REFERENCES AND NOTES

1. D. Chen, S. E. Zebiak, A. J. Busalacchi, M. A. Cane, *Science* **269**, 1699 (1995).
2. M. Ji, A. Leetmaa, V. Kousky, *J. Clim.* **9**, 3105 (1996).
3. M. H. Glantz, *Currents of Change: El Niño's Impact on Climate and Society* (Cambridge Univ. Press, Cambridge, 1996).
4. J. Bjerknes, *Mon. Weather Rev.* **97**, 163 (1969).
5. J. P. McCreary, *ibid.* **111**, 370 (1983).
6. D. S. Battisti, *J. Atmos. Sci.* **45**, 2889 (1988).
7. _____ and A. C. Hirst, *ibid.* **46**, 1687 (1989).
8. P. S. Schopf and M. J. Suarez, *ibid.* **45**, 549 (1988).
9. In this concept, an initial positive SST perturbation in the eastern equatorial Pacific produces a westerly wind anomaly west of the perturbation. This wind anomaly locally enhances the initial SST anomaly through a deepening of the thermocline and generates equatorial upwelling Rossby waves that propagate westward (~0.9 m s^{-1}). According to Bjerknes' concept, the ocean-atmosphere interaction gets into a growing mode and into a fully developed El Niño. The equatorial upwelling Rossby waves reflect on the western ocean boundary as equatorial upwelling Kelvin waves that propagate eastward (~2.7 m s^{-1}) back to the region of positive SST perturbation and counteract its growth.
10. N. J. Mantua and D. S. Battisti, *J. Clim.* **8**, 2897 (1995).
11. T. Delcroix, J.-P. Boulanger, F. Masia, C. Menkes, *J. Geophys. Res.* **99**, 25093 (1994).
12. J.-P. Boulanger and C. Menkes, *ibid.* **100**, 25041 (1995).
13. W. S. Kessler and M. J. McPhaden, *J. Clim.* **8**, 1757 (1995).
14. J.-P. Boulanger and L.-L. Fu, *J. Geophys. Res.* **101**, 16361 (1996).
15. C. Perigaud and B. Dewitte, *J. Clim.* **9**, 66 (1996).
16. M. J. McPhaden and J. Picaut, *Science* **250**, 1385 (1990).
17. N. E. Graham and T. P. Barnett, *J. Clim.* **8**, 544 (1995).
18. J. Picaut and T. Delcroix, *J. Geophys. Res.* **100**, 18393 (1995).
19. J. Picaut, M. Ioualalen, C. Menkes, T. Delcroix, M. J. McPhaden, *Science* **274**, 1486 (1996).
20. In our study, the wave guide was defined by the equatorial band where zonal currents induced by equatorial waves were maxima, 4°N to 4°S or less (*11*). In this band and over the 1986–89 period, there was almost no difference in the zonal displacements of the eastern edge of the warm pool induced by the total zonal surface currents and by the currents restricted to the first baroclinic Kelvin and first meridional Rossby modes (*18*).
21. C. Frankignoul, F. Bonjean, G. Reverdin, *J. Geophys. Res.* **101**, 3629 (1996).
22. M. A. Cane and R. J. Patton, *J. Phys. Oceanogr.* **14**, 1853 (1984).
23. The ocean model covered 130°E to 80°W, 15°N to 15°S, with a 0.5° longitude by 0.125° latitude grid. It was run on a 5-day time step and on an anomaly basis. Dissipation was taken into account in the form of Rayleigh friction. The longitudinal shape of the mean zonal currents was approximated by a simple analytic function, based on drifter observations (*34*) (Fig. 2B).
24. The observed near coincidence of the eastern edge of the warm pool (defined by the 29°C isotherm) and the oceanic zone of current convergence (*19*) was explained by the dominance of zonal advection in the displacements of this edge and the presence there of a nearly constant SST gradient (Fig. 1A).
25. A. E. Gill and E. M. Rasmusson, *Nature* **305**, 229 (1983).
26. A similar concept of expanding wind and zonal displacement of the eastern edge of the warm pool at the onset of an El Niño has been previously modeled [W. S. Kessler, M. J. McPhaden, K. M. Weickmann, *J. Geophys. Res.* **100**, 10613 (1995)].
27. The size and shape of the wind stress patch were determined from observations (Fig. 1D), with meridional and zonal structures approximated by two gaussian functions. The meridional gaussian function was fixed and centered at the equator with about 7° of exponential decay in latitude. The bandwidth of the zonal gaussian function was variable and was set to the distance from OCEE to the midpoint. The change from a constant westerly to a constant easterly during the shift from El Niño to La Niña or vice versa (that is, when the OCEE crosses the midpoint) was done gradually through a cosine function over 10° to 15° longitude. Knowing that anomalous winds due to SST perturbations were located west of these perturbations (Fig. 1, C and D), we shifted the simulated eastern edge of the wind stress patch westward by 5° to 15° compared with the OCEE.
28. The system will forget this initial westerly wind kick once it is on a perpetual ENSO oscillatory motion.
29. Parameters for the standard case were as follows: Kelvin wave speed of 2.8 m s^{-1}, midpoint at 180°, wind trapping in latitude of 7°, westward shift between the eastern edge of the warm pool and that of the wind patch of 10° longitude, wind stress amplitude of 0.33 dyne cm^{-2}, Rayleigh friction of 2 $year^{-1}$, and total currents averaged within 2°N to 2°S with 25 cm s^{-1} and −50 cm s^{-1} for the mean zonal currents near the western and eastern ocean boundary, respectively (Fig. 2B).
30. W. H. Quin, V. T. Neal, S. E. Antunez de Mayolo, *J. Geophys. Res.* **92**, 14449 (1987).
31. T. Delcroix, J. Picaut, G. Eldin, *ibid.* **96**, 3249 (1991).
32. J. Picaut, C. Menkes, J.-P. Boulanger, Y. du Penhoat, *TOGA Notes* **10**, 11 (1993).
33. J. Picaut, F. Masia, Y. du Penhoat, data not shown.
34. P. Niiler *et al.*, *J. Phys. Oceanogr.*, in press.
35. W. T. Liu, A. Zhang, J. K. B. Bishop, *J. Geophys. Res.* **99**, 12623 (1994).
36. In the upper 100 m of the water column and within the wave guide, the variations of transport during El Niño–La Niña events can exceed 50 sverdrups (1 sverdrup = 10^6 m^3 s^{-1}), which is larger than the mean transport of any equatorial currents (*16*). This implies powerful discharge or recharge of water masses in the equatorial band and therefore strong readjustment of the equatorial thermocline together with meridional transfer of water masses [K. Wyrtki, *ibid.* **90**, 7129 (1985)].

37. We thank P. Waigna for preparing all the figures, M. J. Langlade for help in the processing of several figures, and N. J. Mantua and D. S. Battisti for their authorization to reproduce Fig. 1, C and D. The Florida State University wind stress and SST data were provided by J. J. O'Brien and R. W. Reynolds. Discussions and corrections on an early draft by T. Delcroix, P. Rual, L. M. Rothstein, G. Eldin, A. J. Busalacchi, M. J. McPhaden, and J. P. McCreary are appreciated. Supported by ORSTOM, Programme National d'Etudes de la Dynamique du Climat, and Centre National d'Etudes Spatiales.

26 March 1997; accepted 11 June 1997

An Advective-Reflective Conceptual Model for the Oscillatory Nature of the ENSO

J. Picaut, F. Masia and Y. du Penhoat

Science **277** (5326), 663-666.
DOI: 10.1126/science.277.5326.663